

Magneto-transport in mesoscopic rings and cylinders: Effects of electron-electron interaction and spin-orbit coupling

Santanu K. Maiti^{1,*}

¹*School of Chemistry, Tel Aviv University, Ramat-Aviv, Tel Aviv-69978, Israel*

We undertake an in-depth analysis of the magneto-transport properties in mesoscopic single-channel rings and multi-channel cylinders within a tight-binding formalism. The main focus of this review is to illustrate how the long standing anomalies between the calculated and measured current amplitudes carried by a small conducting ring upon the application of a magnetic flux ϕ can be removed. We discuss two different cases. First, we examine the combined effect of second-neighbor hopping integral and Hubbard correlation on the enhancement of persistent current in presence of disorder. A significant change in current amplitude is observed compared to the traditional nearest-neighbor hopping model and the current amplitude becomes quite comparable to experimental realizations. In the other case we verify that in presence of spin-orbit interaction a considerable enhancement of persistent current amplitude takes place, and the current amplitude in a disordered ring becomes almost comparable to that of an ordered one. In addition to these, we also present the detailed band structures and some other related issues to get a complete picture of the phenomena at the microscopic level.

PACS numbers: 73.23.-b, 73.23.Ra, 73.21.Hb

I. INTRODUCTION

The study of magneto-transport properties in low-dimensional systems is always an interesting problem in mesoscopic physics. This is relatively a new branch of condensed matter physics which deals with systems whose dimensions are intermediate between the microscopic and macroscopic length scales¹⁻⁵. In contrast to the macroscopic objects where we generally use the laws of classical mechanics, the meso-scale systems are treated quantum mechanically since in this region fluctuations play the very crucial role. Over the last many years low-dimensional model quantum systems have been the objects of intense research, both in theory and in experiments, mainly due to the fact that these simple looking systems are prospective candidates for nano devices in electronic as well as spintronic engineering⁶⁻²³.

Several striking spectral properties are also exhibited by such systems owing to the quantum interference which is specially observed in quantum geometries with closed loop structures. The existence of dissipationless current in a mesoscopic metallic ring threaded by an Aharonov-Bohm (AB) flux ϕ is a direct consequence of quantum phase coherence. In this new quantum regime, two important aspects appear at low temperatures. The first one is that the phase coherence length L_ϕ i.e., the length scale over which an electron maintains its phase memory, increases significantly with the lowering of temperature and becomes comparable to the system size L . The other one is that the energy levels of such small finite size systems are discrete. These two are the most essential criteria for the appearance of persistent charge current in a small metallic ring/cylinder due to the application of an external magnetic flux ϕ . In the pioneering work of Büttiker, Imry and Landauer²⁴, the appearance of persistent current in metallic rings has been explored. Later, many excellent experiments²⁵⁻³⁰ have been carried out

in several ring and cylindrical geometries to reveal the actual mechanisms of persistent current. Though much efforts have been paid to study persistent current both theoretically³¹⁻⁵³ as well as experimentally²⁵⁻³⁰, yet several anomalies still exist between the theory and experiment, and the full knowledge about it in this scale is not well established even today.

The results of the single loop experiments are significantly different from those for the ensemble of isolated loops. Persistent currents with expected ϕ_0 periodicity have been observed in isolated single Au rings²⁶ and in a GaAs-AlGaAs ring²⁷. Levy *et al.*²⁵ found oscillations with period $\phi_0/2$ rather than ϕ_0 in an ensemble of 10^7 independent Cu rings. Similar $\phi_0/2$ oscillations were also reported for an ensemble of disconnected 10^5 Ag rings²⁹ as well as for an array of 10^5 isolated GaAs-AlGaAs rings³⁰. In a recent experiment, Jariwala *et al.*²⁸ obtained both ϕ_0 and $\phi_0/2$ periodic persistent currents in an array of thirty diffusive mesoscopic Au rings. Except for the case of the nearly ballistic GaAs-AlGaAs ring²⁷, all the measured currents are in general one or two orders of magnitude larger than those expected from the theory.

Free electron theory predicts that at absolute zero temperature ($T = 0$ K), an ordered one-dimensional (1D) metallic ring threaded by magnetic flux ϕ supports persistent current with maximum amplitude $I_0 = ev_F/L$, where v_F is the Fermi velocity and L is the circumference of the ring. Metals are intrinsically disordered which tends to decrease the persistent current, and the calculations show that the disorder-averaged current $\langle I \rangle$ crucially depends on the choice of the ensemble^{32,36,37}. The magnitude of the current $\langle I^2 \rangle^{1/2}$ is however insensitive to the averaging issues, and is of the order of $I_0 l/L$, l being the elastic mean free path of the electrons. This expression remains valid even if one takes into account the finite width of the ring by adding contributions from the transverse channels, since disorder leads to a compensation

between the channels^{32,36}. However, the measurements on an ensemble of 10^7 Cu rings²⁵ reported a diamagnetic persistent current of average amplitude $3 \times 10^{-3} \text{ } ev_F/L$ with half a flux-quantum periodicity. Such $\phi_0/2$ oscillations with diamagnetic response were also found in other persistent current experiments consisting of ensemble of isolated rings^{29,30}.

Measurements on single isolated mesoscopic rings on the other hand detected ϕ_0 -periodic persistent currents with amplitudes of the order of $I_0 \sim ev_F/L$, (closed to the value for an ordered ring). Theory and experiment²⁷ seem to agree only when *disorder is weak*. In another recent nice experiment Bluhm *et al.*⁵⁴ have measured the magnetic response of 33 individual cold mesoscopic gold rings, one ring at a time, using a scanning SQUID technique. They have measured h/e component and predicted that the measured current amplitude agrees quite well with theory³¹ in a single ballistic ring²⁷ and an ensemble of 16 nearly ballistic rings⁵⁵. However, the amplitudes of the currents in single-isolated-diffusive gold rings²⁶ were two orders of magnitude larger than the theoretical estimates. This discrepancy initiated intense theoretical activity, and it is generally believed that the electron-electron correlation plays an important role in the disordered diffusive rings⁴²⁻⁴⁴. An explanation based on the perturbative calculation in presence of interaction and disorder has been proposed and it seems to give a quantitative estimate closer to the experimental results, but still it is less than the measured currents by an order of magnitude, and the interaction parameter used in the theory is not well understood physically.

To remove the controversies regarding the persistent current amplitude between theoretical and experimental verifications we can proceed in two different ways. In literature almost all the theoretical results have been done based on a tight-binding (TB) framework within the *nearest-neighbor hopping* (NNH) approximation. It has been shown that in the NNH model electronic correlation provides a small enhancement of current amplitude in disordered materials i.e., a weak delocalizing effect is observed in presence of electron-electron (e-e) interaction. As a first attempt, we modify the traditional NNH model by incorporating the effects of higher order hopping integrals, at least second-neighbor hopping (SNH), in addition to the NNH integral. It is also quite physical since electrons have some finite probabilities to hop from one site to other sites apart from nearest-neighbor with reduced strengths. We will show that the inclusion of higher order hopping integrals gives significant enhancement of current amplitude and it reaches quite closer to the current amplitude of ordered systems. This is one approach. In the other way we examine that in presence of spin-orbit (SO) interaction a considerable enhancement of persistent current amplitude takes place, and the current amplitude in the disordered ring is almost comparable to that of an ordered ring. The spin-orbit fields in a solid are called the Rashba spin-orbit interaction (RSOI) or the Dresselhaus spin-orbit interaction (DSOI)

depending on whether the electric field originates from a structural inversion asymmetry or the bulk inversion asymmetry respectively⁵⁶. Quantum rings formed at the interface of two semiconducting materials are ideal candidates where the interplay of the two kinds of SOI might be observed. A quantum ring in a heterojunction is realized when a two dimensional gas of electrons is trapped in a quantum well due to the *band offset* at the interface of two different semiconducting materials. This *band offset* creates an electric field which may be described by a potential gradient normal to the interface⁵⁷. The potential at the interface is thus asymmetric, leading to the presence of a RSOI. On the other hand, at such interfaces, the bulk inversion symmetry is naturally broken.

The other important controversy comes for the determination of the sign of low-field currents and still it is an unresolved issue between theoretical and experimental results. In an experiment on persistent current Levy *et al.*²⁵ have shown diamagnetic nature for the measured currents at low-field limit. While, in other experiment Chandrasekhar *et al.*²⁶ have obtained paramagnetic response near zero field limit. Jariwala *et al.*²⁸ have predicted diamagnetic persistent current in their experiment and similar diamagnetic response in the vicinity of zero field limit were also supported in an experiment done by Deblock²⁹ *et al.* on Ag rings. Yu and Fowler⁴⁵ have shown both diamagnetic and paramagnetic responses in mesoscopic Hubbard rings. Though in a theoretical work Cheung *et al.*³² have predicted that the direction of current is random depending on the total number of electrons in the system and the specific realization of the random potentials. Hence, prediction of the sign of low-field currents is still an open challenge and further studies on persistent current in mesoscopic systems are needed to remove the existing controversies.

In the present review we address several important issues of magneto-transport in single-channel mesoscopic rings and multi-channel mesoscopic cylinders which are quite challenging from the standpoint of theoretical as well as experimental research. A brief outline of the presentation is as follows.

First, we address magnetic response in mesoscopic Hubbard rings threaded by AB flux ϕ . We try to propose an idea to remove the unexpected discrepancy between the calculated and measured current amplitudes by incorporating the effect of second-neighbor hopping (SNH) in addition to the traditional nearest-neighbor hopping (NNH) integral in the tight-binding Hamiltonian. Using a generalized Hartree-Fock (HF) approximation⁵⁸⁻⁶², we numerically compute persistent current (I), Drude weight (D) and low-field magnetic susceptibility (χ) as functions of AB flux ϕ , total number of electrons N_e and system size N . With this (HF) approach one can study magnetic response in a much larger system since here a many-body Hamiltonian is decoupled into two effective one-body Hamiltonians. One is associated with up spin electrons and other is related to down spin electrons. But the point is that, the results calculated using gener-

alized HF mean-field theory may deviate from exact results with the reduction of dimensionality. So we should take care about the mean-field calculation, specially, in 1D systems. To trust our predictions, here we also make a comparative study between the results obtained from mean-field theory and exactly diagonalizing the full many-body Hamiltonian. The later approach where a complete many-body Hamiltonian is diagonalized to get energy eigenvalues is not suitable to study magnetic response in larger systems since the size of the matrices increases very sharply with the total number of up and down spin electrons.

Next, we explore the behavior of persistent current in an interacting mesoscopic ring with finite width threaded by an Aharonov-Bohm flux ϕ . For this cylindrical system we also see that the inclusion of higher order hopping integrals leads to a possibility of getting enhanced persistent current and the current is quite comparable to the ordered one. Our results can be utilized to study magnetic response in any interacting mesoscopic system.

Finally, in the last part, we focus our attention on the behavior of persistent current in a one-dimensional mesoscopic ring threaded by a magnetic flux in presence of the Rashba and Dresselhaus SO interactions. Here, the effect of electron-electron interaction is neglected. We show that the presence of the SO interaction leads to a significant enhancement of persistent current⁶³. In addition to these, we also describe very briefly the energy band structures and the oscillations of persistent current as the RSOI is varied to make the present communication a self contained study.

Throughout the review we perform all the essential features of magneto-transport at absolute zero temperature and set $c = e = h = 1$ for numerical calculations.

II. A HUBBARD RING IN ABSENCE OF SO INTERACTIONS

In this section we describe the magneto-transport properties in a single-channel 1D mesoscopic ring in the presence of on-site Coulomb interaction. The effect of SO interaction is not taken into account.

A. Model and theoretical formulation

We start by referring to Fig. 1, where a normal metal ring is threaded by a magnetic flux ϕ . To describe the system we use a tight-binding framework. For a N -site ring, penetrated by a magnetic flux ϕ (measured in unit of the elementary flux quantum $\phi_0 = ch/e$), the tight-binding Hamiltonian in Wannier basis looks in the form,

$$H_R = \sum_{i,\sigma} \epsilon_{i\sigma} c_{i\sigma}^\dagger c_{i\sigma} + \sum_{ij,\sigma} t \left[e^{i\theta} c_{i\sigma}^\dagger c_{j\sigma} + h.c. \right] + \sum_{ik,\sigma} t_1 \left[e^{i\theta_1} c_{i\sigma}^\dagger c_{k\sigma} + h.c. \right] + \sum_i U c_{i\uparrow}^\dagger c_{i\uparrow} c_{i\downarrow}^\dagger c_{i\downarrow} \quad (1)$$

where, $\epsilon_{i\sigma}$ is the on-site energy of an electron at the site i of spin σ (\uparrow, \downarrow). The variable t corresponds to the nearest-neighbor ($j = i \pm 1$) hopping strength, while t_1 gives the second-neighbor ($k = i \pm 2$) hopping integral. $\theta = 2\pi\phi/N$ and $\theta_1 = 4\pi\phi/N$ are the phase factors associated with the hopping of an electron from one site to its neighboring site and next-neighboring site, respectively. $c_{i\sigma}^\dagger$ and $c_{i\sigma}$

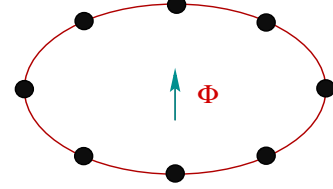


FIG. 1: (Color online). Schematic view of a 1D mesoscopic ring penetrated by a magnetic flux ϕ . The filled black circles correspond to the positions of the atomic sites.

are the creation and annihilation operators, respectively, of an electron at the site i with spin σ . U is the strength of on-site Hubbard interaction.

Decoupling of the interacting Hamiltonian: In order to determine the energy eigenvalues of the interacting model quantum system described by the tight-binding Hamiltonian given in Eq. 1, first we decouple the interacting Hamiltonian using generalized Hartree-Fock approach, the so-called mean field approximation. In this approach, the full Hamiltonian is completely decoupled into two parts. One is associated with the up-spin electrons, while the other is related to the down-spin electrons with their modified site energies. For up and down spin Hamiltonians, the modified site energies are expressed in the form, $\epsilon'_{i\uparrow} = \epsilon_{i\uparrow} + U\langle n_{i\downarrow} \rangle$ and $\epsilon'_{i\downarrow} = \epsilon_{i\downarrow} + U\langle n_{i\uparrow} \rangle$, where $n_{i\sigma} = c_{i\sigma}^\dagger c_{i\sigma}$ is the number operator. With these site energies, the full Hamiltonian (Eq. 1) can be written in the decoupled form as,

$$\begin{aligned} H_R &= \sum_i \epsilon'_{i\uparrow} n_{i\uparrow} + \sum_{ij} t \left[e^{i\theta} c_{i\uparrow}^\dagger c_{j\uparrow} + e^{-i\theta} c_{j\uparrow}^\dagger c_{i\uparrow} \right] \\ &+ \sum_{ik} t_1 \left[e^{i\theta_1} c_{i\uparrow}^\dagger c_{k\uparrow} + e^{-i\theta_1} c_{k\uparrow}^\dagger c_{i\uparrow} \right] \\ &+ \sum_i \epsilon'_{i\downarrow} n_{i\downarrow} + \sum_{ij} t \left[e^{i\theta} c_{i\downarrow}^\dagger c_{j\downarrow} + e^{-i\theta} c_{j\downarrow}^\dagger c_{i\downarrow} \right] \\ &+ \sum_{ik} t_1 \left[e^{i\theta_1} c_{i\downarrow}^\dagger c_{k\downarrow} + e^{-i\theta_1} c_{k\downarrow}^\dagger c_{i\downarrow} \right] \\ &- \sum_i U \langle n_{i\uparrow} \rangle \langle n_{i\downarrow} \rangle \\ &= H_\uparrow + H_\downarrow - \sum_i U \langle n_{i\uparrow} \rangle \langle n_{i\downarrow} \rangle \end{aligned} \quad (2)$$

where, H_\uparrow and H_\downarrow correspond to the effective tight-binding Hamiltonians for the up and down spin electrons, respectively. The last term is a constant term which provides an energy shift in the total energy.

Self consistent procedure: With these decoupled Hamiltonians (H_\uparrow and H_\downarrow) of up and down spin electrons, we start our self consistent procedure considering initial guess values of $\langle n_{i\uparrow} \rangle$ and $\langle n_{i\downarrow} \rangle$. For these initial set of values of $\langle n_{i\uparrow} \rangle$ and $\langle n_{i\downarrow} \rangle$, we numerically diagonalize the up and down spin Hamiltonians. Then we calculate a new set of values of $\langle n_{i\uparrow} \rangle$ and $\langle n_{i\downarrow} \rangle$. These steps are repeated until a self consistent solution is achieved.

Calculation of ground state energy: Using the self consistent solution, the ground state energy E_0 for a particular filling at absolute zero temperature ($T = 0$ K) can be determined by taking the sum of individual states up to Fermi energy (E_F) for both up and down spins. Thus, we can write the final form of ground state energy as,

$$E_0 = \sum_n E_{n\uparrow} + \sum_n E_{n\downarrow} - \sum_i U \langle n_{i\uparrow} \rangle \langle n_{i\downarrow} \rangle \quad (3)$$

where, the index n runs for the states upto the Fermi level. $E_{n\uparrow}$ ($E_{n\downarrow}$) is the single particle energy eigenvalue for n -th eigenstate obtained by diagonalizing the Hamiltonian H_\uparrow (H_\downarrow).

Calculation of persistent current: At absolute zero temperature, total persistent current of the system is obtained from the expression,

$$I(\phi) = -c \frac{\partial E_0(\phi)}{\partial \phi} \quad (4)$$

where, $E_0(\phi)$ is the ground state energy.

Calculation of Drude weight: The Drude weight for the ring can be calculated through the relation,

$$D = \frac{N}{4\pi^2} \left(\frac{\partial^2 E_0(\phi)}{\partial \phi^2} \right) \Big|_{\phi \rightarrow 0} \quad (5)$$

where, N gives total number of atomic sites in the ring. Kohn⁶⁴ has shown that for an insulating system D decays exponentially to zero, while it becomes finite for a conducting system.

Determination of low-field magnetic susceptibility: The general expression of magnetic susceptibility χ at any flux ϕ is written in the form,

$$\chi(\phi) = \frac{N^3}{16\pi^2} \left(\frac{\partial I(\phi)}{\partial \phi} \right). \quad (6)$$

Evaluating the sign of $\chi(\phi)$ we can able to predict whether the current is paramagnetic or diamagnetic in nature. Here we will determine $\chi(\phi)$ only in the limit $\phi \rightarrow 0$, since we are interested to know the magnetic response in the low-field limit.

B. Numerical results and discussion

In this sub-section throughout our numerical work we set the nearest-neighbor hopping strength $t = -1$ and second-neighbor hopping strength $t_1 = -0.7$. Energy scale is measured in unit of t .

1. Perfect Hubbard Rings Described with NNH Integral

For perfect rings we choose $\epsilon_{i\uparrow} = \epsilon_{i\downarrow} = 0$ for all i and since here we consider the rings with only NNH integral, the second-neighbor hopping strength t_1 is fixed at zero.

Energy-flux characteristics: To explain the relevant features of magnetic response we begin with the energy-flux characteristics. As illustrative examples, in Fig. 2 we plot the ground state energy levels as a function of magnetic flux ϕ for some typical mesoscopic rings in the half-filled case, where (a) and (b) correspond to $N = 5$ and 6, respectively. The red curves represent the en-

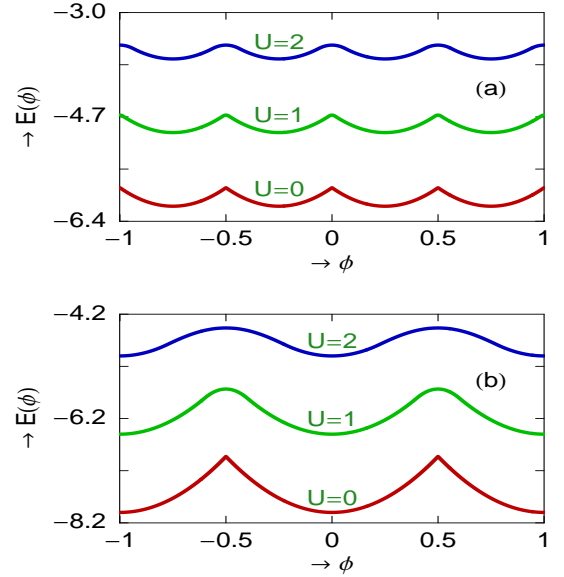


FIG. 2: (Color online). Ground state energy levels as a function of flux ϕ for some typical mesoscopic rings in half-filled case. The red, green and blue curves correspond to $U = 0, 1$ and 2, respectively. (a) $N = 5$ and (b) $N = 6$.

ergy levels for the non-interacting ($U = 0$) rings, while the green and blue lines correspond to the energy levels for the interacting rings where the electronic correlation strength U is fixed to 1 and 2, respectively. From the spectra it is observed that the ground state energy level shifts towards the positive energy and it becomes much flatter with the increase of the correlation strength U . Both for the two different ring sizes ($N = 5$ and 6) the ground state energy levels vary periodically with AB flux ϕ , but a significant difference is observed in their periodicities depending on the oddness and evenness of the ring size N . For $N = 6$ (even), the energy levels show conventional ϕ_0 ($= 1$, in our chosen unit system $c = e = \hbar = 1$) flux-quantum periodicity. On the other hand, the period becomes half i.e., $\phi_0/2$ for $N = 5$ (odd). This $\phi_0/2$ periodicity disappears as long as the filling is considered away from the half-filling. At the same time, it also vanishes if impurities are introduced in the system, even if the ring is half-filled with odd N . Therefore, $\phi_0/2$ periodicity is

a special feature for odd half-filled perfect rings irrespective of the Hubbard strength U , while for all other cases traditional ϕ_0 periodicity is obtained.

To judge the accuracy of the mean-field calculations in our ring geometry, in Fig. 3 we show the variation of lowest energy levels where the eigenenergies are determined through exact diagonalization of the full many-body Hamiltonian for the identical rings as given in

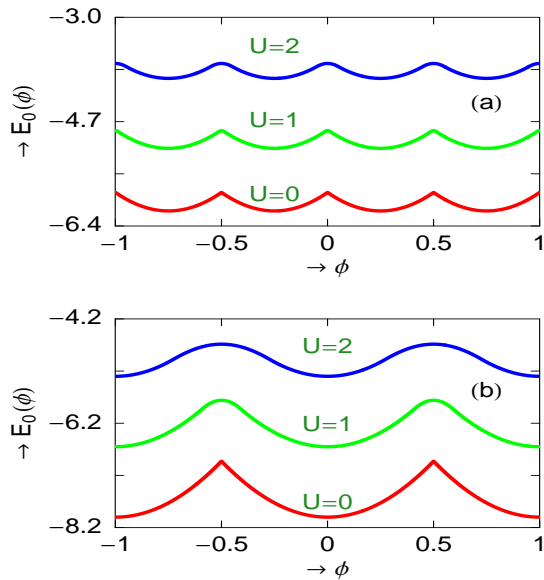


FIG. 3: (Color online). Ground state energy levels as a function of flux ϕ for some typical mesoscopic rings in half-filled case, where eigenenergies are determined through exact diagonalization of the full many-body Hamiltonian. The red, green and blue curves correspond to $U = 0, 1$ and 2 , respectively. (a) $N = 5$ and (b) $N = 6$.

Fig. 2, considering the same parameter values. Comparing the results presented in Figs. 2 and 3, we see that the mean-field results agree very well with the exact diagonalization method. Thus we can safely use mean-field approach to study magnetic response in our geometry.

Current-flux characteristics: Following the above energy-flux characteristics now we describe the behavior of persistent current in mesoscopic Hubbard rings. As representative examples, in Fig. 4 we display the variation of persistent currents as a function of flux ϕ for some typical single-channel mesoscopic rings in the half-filled case, where (a) and (b) correspond to $N = 15$ and 20 , respectively. The red, green and blue curves in Fig. 4(a) correspond to the currents for $U = 0, 1.5$ and 2 , respectively, while these curves in Fig. 4(b) represent the currents for $U = 0, 1$ and 1.5 , respectively. In the absence of any e-e interaction ($U = 0$), persistent current shows saw-tooth like nature as a function of flux ϕ with sharp transitions at $n\phi_0/2$ (red line of Fig. 4(a)) or $n\phi_0$ (red line of Fig. 4(b)), where n being an integer, depending on whether N is odd or even. The saw-tooth

like behavior disappears as long as the electronic correlation is introduced into the system. This is clearly observed from the green and blue curves of Fig. 4. Additionally, in the presence of U , the current amplitude gets suppressed compared to the current amplitude in the non-interacting case, and it decreases gradually with increasing U . This provides the lowering of electron mo-

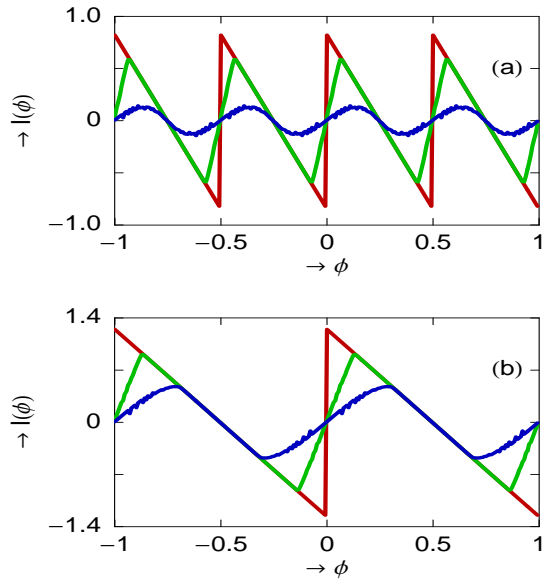


FIG. 4: (Color online). Persistent current as a function of flux ϕ for single-channel mesoscopic rings in half-filled case. (a) $N = 15$. The red, green and blue curves correspond to $U = 0, 1.5$ and 2 , respectively. (b) $N = 20$. The red, green and blue curves correspond to $U = 0, 1$ and 1.5 , respectively.

bility with the rise of U and the reason behind this can be much better understood from our forthcoming discussion. Both for two different rings with sizes $N = 15$ (odd) and 20 (even), persistent currents vary periodically with AB flux ϕ showing different periodicities, following the energy-flux characteristics. For $N = 15$, current shows $\phi_0/2$ flux-quantum periodicity, while for the other case ($N = 20$), current exhibits ϕ_0 flux-quantum periodicity.

Variation of electronic mobility-Drude weight: To reveal the conducting properties of Hubbard rings, we study the variation of Drude weight D for these systems. Drude weight can be calculated by using Eq. 5. Finite value of D predicts the metallic phase, while for the insulating phase it drops exponentially to zero⁶⁴.

As illustrative examples, in Fig. 5 we show the variation of Drude weight D as a function of electronic correlation strength U for some typical single-channel Hubbard rings. In Fig. 5(a) the results are shown for three different half-filled rings, where the red, green and blue lines correspond to the rings with $N = 10, 30$ and 50 , respectively. From the curves it is evident that for smaller values of U , the half-filled rings show finite value of D which reveals that they are in the metallic phase. On the other hand,

D drops sharply to zero when U becomes high. Thus the rings become insulating when U is quite large. The results for the non-half filled case are shown in Fig. 5(b), where we fix the ring size $N = 20$ and vary the electron filling. The red, green and blue curves represent $N_e = 10$, 14 and 18, respectively, where N_e gives the total number of electrons in the ring. For these three choices of N_e , the ring is always less than half-filled (since $N_e < N$) and the ring is in the conducting phase irrespective of

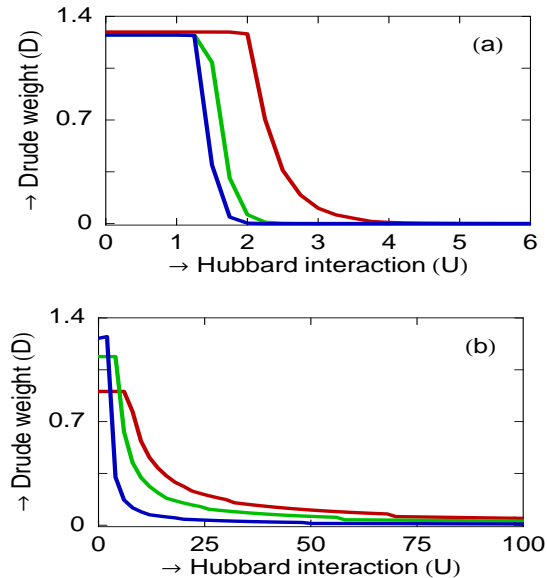


FIG. 5: (Color online). Drude weight as a function of Hubbard interaction strength U for single-channel mesoscopic rings. (a) Half-filled case. The red, green and blue curves correspond to $N = 10$, 30 and 50, respectively. (b) Non-half-filled case with $N = 20$. The red, green and blue curves correspond to $N_e = 10$, 14 and 18, respectively.

the correlation strength U . Now we try to justify the dependence of the Hubbard strength U on the electronic mobility for these different fillings. To understand the effect of U on electron mobility here we measure a quantity called ‘average spin density’ (ASD) which is defined by the factor $\sum_i |(n_{i\uparrow} - n_{i\downarrow})|/N$. The integer i is the site index and it runs from 1 to N . By calculating ASD we can estimate the occupation probability of electrons in the ring and it supports us to explain whether the ring lies in the metallic phase or in the insulating one. For the rings those are below half-filled, ASD is always less than unity irrespective of the value of U as shown by the curves in Fig. 6(b). It reveals that for these systems, ground state always supports an empty site and electron can move along the ring avoiding double occupancy of two different spin electrons at any site i in the presence of e-e correlation which provides the metallic phase ($D > 0$). For a fixed ring size and a particular strength of U , the ASD increases as the filling is increased towards half-filling which is noticed by comparing the three different curves in Fig. 6(b). On the other hand, in the

half-filled rings, ASD is less than unity for small value of U , while it reaches to unity when U is large. This behavior is clearly shown by the curves given in Fig. 6(a), where the red, green and blue lines correspond to ASDs for the half-filled rings with $N = 10$, 30 and 50, respectively. Thus, for low U there is some finite probability of getting two opposite spin electrons in a same site which allows electrons to move along the ring and the metallic phase is obtained. But for large U , ASD reaches to unity

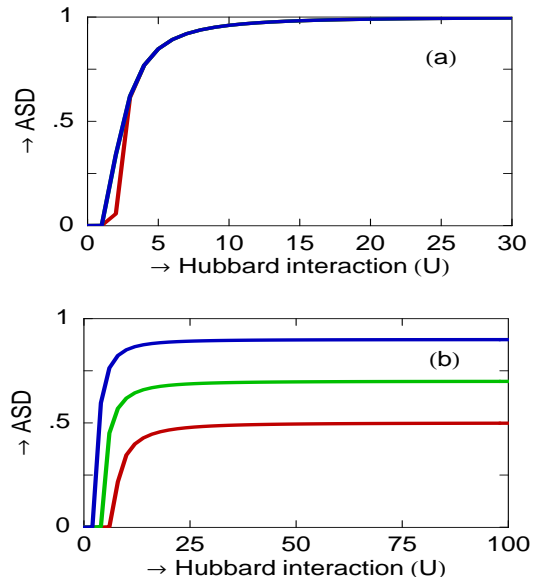


FIG. 6: (Color online). Average spin density (ASD) as a function of Hubbard interaction strength U for single-channel mesoscopic rings. (a) Half-filled case. The red, green and blue curves correspond to $N = 10$, 30 and 50, respectively. (b) Non-half-filled case with $N = 20$. The red, green and blue curves correspond to $N_e = 10$, 14 and 18, respectively.

which means that each site is singly occupied either by an up or down spin electron with probability 1. In this case ground state does not support any empty site and due to strong repulsive e-e correlation one electron sitting in a site does not allow to come other electron with opposite spin from the neighboring site which provides the insulating phase ($D = 0$). The situation is somewhat analogous to Mott localization in one-dimensional infinite lattices. In perfect Hubbard rings the conducting nature has been studied exactly quite a long ago using the ansatz of Bethe by Shastri and Sutherland⁶⁵. They have calculated charge stiffness constant (D_c) and have predicted that D_c goes to zero as the system approaches towards half-filling for any non-zero value of U . Our numerical results clearly justify their findings.

Low-field magnetic susceptibility: Now, we discuss the variation of low-field magnetic susceptibility which can be calculated from Eq. 6 by setting $\phi \rightarrow 0$. With the help of this parameter we can justify whether the current is paramagnetic (+ve slope) or diamagnetic (−ve

slope) in nature. For our illustrative purposes, in Fig. 7 we show the variation of low-field magnetic susceptibility with system size N for some typical single-channel mesoscopic rings in the half-filled case. Figure 7(a) correspond to the variation of low-field magnetic susceptibility for the non-interacting ($U = 0$) rings, where the

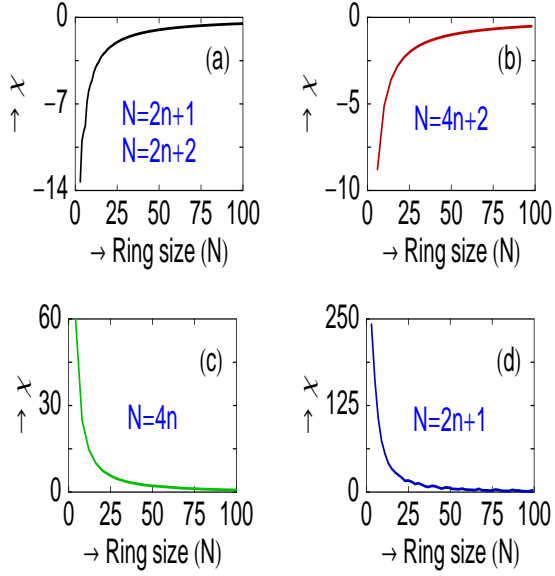


FIG. 7: (Color online). Low-field magnetic susceptibility as a function of system size N for single-channel mesoscopic rings in half-filled case. (a) $U = 0$. N is an odd ($2n + 1$) or an even ($2n + 2$) number, where n is an integer. (b) $U = 1$. N is an even number obeying the relation $N = 4n + 2$. (c) $U = 1$. N is an even number satisfying the relation $N = 4n$. (d) $U = 1$. N is an odd number following the relation $N = 2n + 1$.

ring size can be anything i.e., either odd, following the relation $N = 2n + 1$ (n is an integer), or even, obeying the expression $N = 2n + 2$. It is observed that both for odd and even N , low-field current exhibits diamagnetic nature. The behavior of the low-field currents changes significantly when the e-e interaction is taken into account. Depending on the ring size N , the sign becomes +ve and -ve as shown by the curves given in Figs. 7(b)-(d). For the interacting rings where the relation $N = 4n + 2$ is satisfied, the low-field current becomes diamagnetic (Fig. 7(b)). The sign becomes paramagnetic when $N = 4n$ (Fig. 7(c)) and $N = 2n + 1$ (Fig. 7(d)). Thus, in brief, we say that for non-interacting half-filled rings low-field current exhibits diamagnetic response irrespective of N i.e., whether N is odd or even. For the interacting half-filled rings with odd N , low-field current provides only the paramagnetic behavior, while for even N , depending on the particular value of N , the response becomes either diamagnetic or paramagnetic. These natures of low-field currents change for the cases of other electron fillings. Hence, it can be emphasized that the behavior of the low-field currents is highly sensitive on the Hubbard correlation, electron filling, evenness and odd-

ness of N , etc. The behavior of zero-field magnetic susceptibility in Hubbard rings has been studied extensively quite a long back using the Bethe ansatz by Shiba⁶⁶. In this work, he has studied magnetic susceptibility per electron as functions of electron filling and Hubbard correlation strength and provided several interesting results. From his findings we can clearly justify our presented results.

2. Disordered Hubbard Rings Described with NNH and SNH Integrals

Now, we explore the combined effect of electron-electron correlation and second-neighbor hopping (SNH) integral on persistent current in disordered mesoscopic rings.

To get a disordered ring, we choose site energies ($\epsilon_{i\uparrow}$ and $\epsilon_{i\downarrow}$) randomly from a “Box” distribution function of width W . As the site energies are chosen randomly it is needed to consider the average over a large number of disordered configurations (from the stand point of statistical average). Here, we determine the currents by taking the average over 50 random disordered configuration in each case to achieve much accurate results.

As illustrative examples, in Fig. 8 we display the variation of persistent currents for some single-channel mesoscopic rings considering 1/3 electron filling. In (a) the results are given for the rings characterized by the NNH integral model. The red curve represents the current for the ordered ($W = 0$) non-interacting ($U = 0$) ring. It shows saw-tooth like nature with AB flux ϕ providing ϕ_0 flux-quantum periodicity. The situation becomes completely different when impurities are introduced in the ring as clearly seen by the other two colored curves. The green curve represents the current for the case only when impurities are considered but the effect of Hubbard interaction is not taken into account. It varies continuously with ϕ and gets much reduced amplitude, even an order of magnitude, compared to the perfect case. This is due to the localization of the energy eigenstates in the presence of impurity, which is the so-called Anderson localization. Hence, a large difference exists between the current amplitudes of an ordered and disordered non-interacting rings and it was the main controversial issue among the theoretical and experimental predictions. Experimental results suggest that the measured current amplitude is quite comparable to the theoretically estimated current amplitude in a perfect system. To remove this controversy, as a first attempt, we include the effect of Hubbard interaction in the disordered ring described by the NNH model. The result is shown by the blue curve where U is fixed at 0.5. It is observed that the current amplitude gets increased compared to the non-interacting disordered ring, though the increment is too small. Not only that the enhancement can take place only for small values of U , while for large enough U the current amplitude rather decreases. This phenomenon

can be explained as follows. For the non-interacting disordered ring the probability of getting two opposite spin electrons becomes higher at the atomic sites where the site energies are lower than the other sites since the electrons get pinned at the lower site energies to minimize the ground state energy, and this pinning of electrons becomes increased with the rise of impurity strength W . As a result the mobility of electrons and hence the current amplitude gets reduced with the increase of impurity strength W . Now, if we introduce electronic correlation in the system then it tries to depin two opposite spin electrons those are situated together due to the Coulomb repulsion. Therefore, the electronic mobility is enhanced which provides quite larger current amplitude. But, for

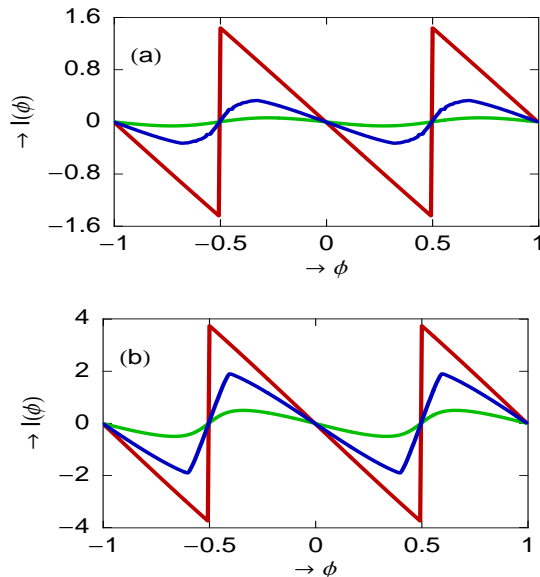


FIG. 8: (Color online). Persistent current as a function of flux ϕ for single-channel mesoscopic rings with $N = 15$ considering $1/3$ electron filling. (a) Rings with only NNH integral. The red line corresponds to the ordered non-interacting ring, while the green and blue lines correspond to the disordered ($W = 2$) rings with $U = 0$ and 0.5 , respectively. (b) Rings with NNH and SNH integrals. The red line represents the ordered non-interacting ring, whereas the green and blue line correspond to the disordered ($W = 2$) rings with $U = 0$ and 1.5 , respectively.

large enough interaction strength, mobility of electrons gradually decreases due to the strong repulsive interaction. Accordingly, the current amplitude gradually decreases with U . So, in short, we can say that within the nearest-neighbor hopping (NNH) model electron-electron interaction does not provide any significant contribution to enhance the current amplitude, and hence the controversy regarding the current amplitude still persists.

To overcome this controversy, finally we make an attempt by incorporating the effect of second-neighbor hopping (SNH) integral in addition to the nearest-neighbor hopping (NNH) integral. With this modification a significant change in current amplitude takes place which

is clearly observed from Fig. 8(b). The red curve refers to the current for the perfect ($W = 0$) non-interacting ($U = 0$) ring and it achieves much higher amplitude compared to the NNH model (see red curve of Fig. 8(a)). This additional contribution comes from the SNH integral since it allows electrons to hop further. The main focus of this sub-section is to interpret the combined effect of SNH integral and Hubbard correlation on the enhancement of persistent current in disordered ring. To do this first we narrate the effect of SNH integral in disordered non-interacting ring. The nature of the current for this particular case is shown by the green curve of Fig. 8(b). It shows that the current amplitude gets reduced compared to the perfect case (red line), which is expected, but the reduction of the current amplitude is very small than the NNH integral model (see green curve of Fig. 8(a)). This is due the fact that the SNH integral tries to delocalize the electronic states, and therefore, the mobility of the electrons is enriched. The situation becomes more interesting when we include the effect of Hubbard interaction. The behavior of the current in the presence of interaction is plotted by the blue curve of Fig. 8(b) where we fix $U = 1.5$. Very interestingly we see that the current amplitude is enhanced moderately and quite comparable to that of the perfect ring. Therefore, it can be predicted that the presence of SNH integral and Hubbard interaction can provide a persistent current which may be comparable to the measured current amplitudes. In the above analysis we consider the effect of only SNH integral in addition to the NNH model, and, illustrate how such a higher order hopping integral leads to an important role on the enhancement of current amplitude in presence of Hubbard correlation for disordered rings. Instead of considering only the SNH integral we can also take the contributions from all possible higher order hopping integrals with reduced hopping strengths. Since the strengths of other higher order hopping integrals are too small, the contributions from these factors are reasonably small and they will not provide any significant change in the current amplitude.

III. A HUBBARD CYLINDER IN ABSENCE OF SO INTERACTIONS

In this section we extend our discussion for an interacting mesoscopic ring with finite width threaded by an AB flux ϕ . Here also we ignore the effect of SO interaction on magneto-transport properties like the previous section.

A. Model and the Hamiltonian

Let us start by referring to Fig. 9, where a small metallic cylinder is threaded by a magnetic flux ϕ . The filled black circles correspond to the positions of the atomic sites in the cylinder. To predict the size of a cylinder we

use two parameters N and M , where the 1st one (N) represents total number of atomic sites in each circular ring and the other one (M) gives total number of identical circular rings. For the description of our model quantum system we use a tight-binding framework and in order to incorporate the effect of higher order hopping integrals to the Hamiltonian here we consider second-neighbor hopping (SNH) (shown by the red dashed line in Fig. 9) in addition to the nearest-neighbor hopping (NNH) of elec-

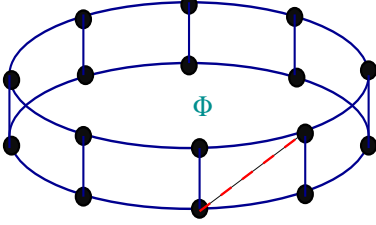


FIG. 9: (Color online). Schematic view of a 1D mesoscopic cylinder penetrated by a magnetic flux ϕ . The red dashed line corresponds to the second-neighbor hopping integral and the filled black circles represent the positions of the atomic sites. A persistent current I is established in the cylinder.

trons. Considering both NNH and SNH integrals the TB Hamiltonian for the cylindrical system in Wannier basis looks in the form,

$$\begin{aligned}
 H_C = & \sum_{i,j,\sigma} \epsilon_{i,j,\sigma} c_{i,j,\sigma}^\dagger c_{i,j,\sigma} + \sum_{i,j,\sigma} t_l \left[e^{i\theta_l} c_{i,j,\sigma}^\dagger c_{i,j+1,\sigma} \right. \\
 & + \left. h.c. \right] + \sum_{i,j,\sigma} t_d \left[e^{i\theta_d} c_{i,j,\sigma}^\dagger c_{i+1,j+1,\sigma} + h.c. \right] \\
 & + \sum_{ij} U c_{i,j,\uparrow}^\dagger c_{i,j,\uparrow} c_{i,j,\downarrow}^\dagger c_{i,j,\downarrow}
 \end{aligned} \quad (7)$$

where, (i, j) represent the co-ordinate of a lattice site. The index i runs from 1 to M , while the integer j goes from 1 to N . $\epsilon_{i,j,\sigma}$ is the on-site energy of an electron at the site (i, j) of spin σ (\uparrow, \downarrow). t_l and t_d are the NNH and SNH integrals, respectively. Due to the presence of magnetic flux ϕ (measured in unit of the elementary flux quantum $\phi_0 = ch/e$), a phase factor $\theta_l = 2\pi\phi/N$ appears in the Hamiltonian when an electron hops longitudinally from one site to its neighboring site, and accordingly, a negative sign comes when the electron hops in the reverse direction. θ_d is the associated phase factor for the diagonal motion of an electron between two neighboring concentric rings. No phase factor appears when an electron moves along the vertical direction which is set by proper choice of the gauge for the vector potential \vec{A} associated with the magnetic field \vec{B} , and this choice makes the phase factors (θ_l, θ_d) identical to each other for the longitudinal and diagonal motions. Since the magnetic field corresponding to the AB flux ϕ does not penetrate anywhere of the surface of the cylinder, we ignore Zeeman term in the above tight-binding Hamiltonian (Eq. 7). $c_{i,j,\sigma}^\dagger$ and $c_{i,j,\sigma}$ are the creation and annihilation oper-

ators, respectively, of an electron at the site (i, j) with spin σ . U is the on-site Hubbard interaction term.

B. Theoretical formulation

To calculate energy eigenvalues, persistent current and related issues here we follow exactly the same prescription which we illustrate in the earlier section (Sec. II) i.e., Hartree-Fock mean-field approach.

C. Numerical results and discussion

Throughout the numerical analysis, in this sub-section, we set the nearest-neighbor hopping strength $t_l = -1$ and fix $M = 2$ i.e., cylinders with two identical rings. Energy scale is measured in the unit of t_l . We describe the results in three different parts. In the first part, we consider perfect cylinders with only nearest-neighbor hopping integral. In the second part, disordered cylinders described with only NNH integral are considered. Finally, in the third part we discuss the effect of second-neighbor hopping (SNH) integral on the enhancement of persistent current in disordered cylinders.

1. Perfect cylinders with NNH integral

For perfect cylinders we choose $\epsilon_{i,j,\uparrow} = \epsilon_{i,j,\downarrow} = 0$ for all (i, j) . Since here we consider the cylinders described with NNH integral only, the second-neighbor hopping strength t_d is fixed to zero.

Energy-flux characteristics: As illustrative examples, in Fig. 10 we show the variation of ground state energy levels as a function of magnetic flux ϕ for some typical mesoscopic cylinders where N is fixed at 5 (odd N). In (a) the results are given for the quarterly-filled ($N_e = 5$) cylinders, while in (b) the curves correspond to the results for the half-filled ($N_e = 10$) cylinders. The red, green and blue lines represent the ground state energy levels for $U = 0, 0.5$ and 1 , respectively. It is observed that the ground state energy shows oscillatory behavior as a function of ϕ and the energy increases as the electronic correlation strength U gets increased. Most significantly we see that the ground state energy levels provide two different types of periodicities depending on the electron filling. At quarter-filling, ground state energy level gives ϕ_0 ($= 1$, since $c = e = h = 1$ in our chosen unit system) flux-quantum periodicity. On the other hand, at half-filling it shows $\phi_0/2$ flux-quantum periodicity. The situation becomes quite different when the total number of atomic sites N in individual rings is even. For our illustrative purposes in Fig. 11 we plot the lowest energy levels as a function of ϕ for some typical mesoscopic cylinders considering $N = 8$ (even N). The curves of different colors correspond to the identical meaning as in

Fig. 10. From the spectra given in Figs. 11(a) (quarter-filled case) and (b) (half-filled case) it is clearly observed that the ground state energy levels vary periodically with

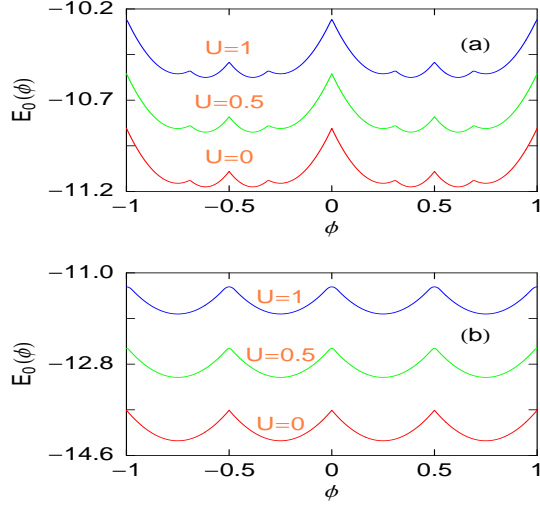


FIG. 10: (Color online). Ground state energy levels as a function of flux ϕ for some perfect cylinders with $N = 5$ and $M = 2$. The red, green and blue curves correspond to $U = 0, 0.5$ and 1 , respectively. (a) Quarter-filled case and (b) Half-filled case.

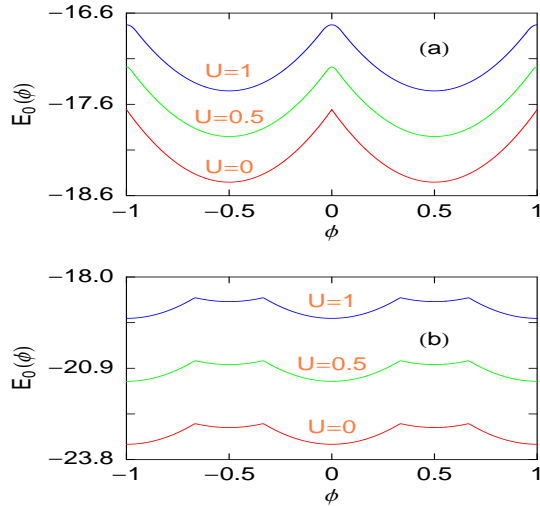


FIG. 11: (Color online). Ground state energy levels as a function of flux ϕ for some perfect cylinders considering $N = 8$ and $M = 2$. The red, green and blue curves correspond to $U = 0, 0.5$ and 1 , respectively. (a) Quarter-filled case and (b) Half-filled case.

AB flux ϕ exhibiting only ϕ_0 flux-quantum periodicity. Thus it can be emphasized that the appearance of half flux-quantum periodicity strongly depends on the electron filling as well as on the oddness and evenness of the total number of atomic sites N in individual rings. Only for the half-filled cylinders with odd N , the lowest energy

level gets $\phi_0/2$ periodicity with flux ϕ . Now it is important to note that this half flux-quantum periodicity does not depend on the width (M) of the cylinder and also it is independent of the Hubbard correlation strength U . Hence, depending on the system size and filling of electrons variable periodicities are observed in the variation of lowest energy level. It may provide an important signature in studying magnetic response in nano-scale loop geometries.

Current-flux characteristics: In Fig. 12 we display the current-flux characteristics for some impurity free mesoscopic cylinders considering $M = 2$. In (a) the results are given for the half-filled case where we set

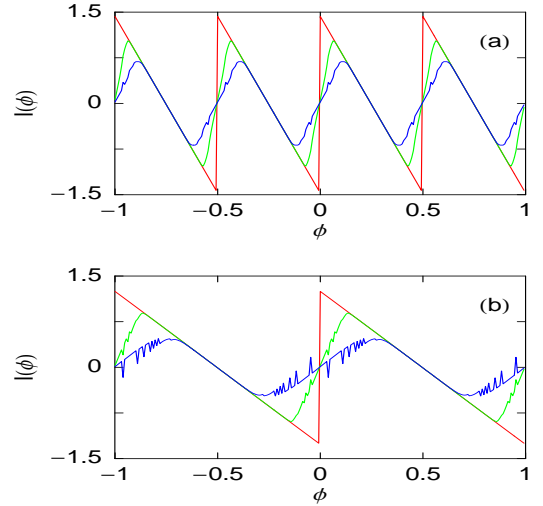


FIG. 12: (Color online). Persistent current as a function of flux ϕ for some ordered mesoscopic cylinders considering $M = 2$. (a) Half-filled case with $N = 15$. The red, green and blue curves correspond to $U = 0, 1.5$ and 2 , respectively. (b) Quarter-filled case with $N = 20$. The red, green and blue curves correspond to $U = 0, 2$ and 3 , respectively.

$N = 15$. The red line corresponds to the current for the non-interacting ($U = 0$) case, while the green and blue lines represent the currents when $U = 1.5$ and 2 , respectively. From the curves we notice that the current amplitude gradually decreases with the increase of electronic correlation strength U . The reason is that at half-filling each site is occupied by at least one electron of up spin or down spin, and the placing of a second electron of opposite spin needs more energy due to the repulsive effect of U . Thus conduction becomes difficult as it requires more energy when an electron hops from its own site and situates at the neighboring site. Now both for the non-interacting and interacting cases, current shows half flux-quantum periodicity as a function a ϕ obeying the energy-flux characteristics since here we choose odd N ($N = 15$). The behavior of the persistent currents for even N is shown in (b) where we set $N = 20$. The currents are drawn for the quarter-filled case i.e., $N_e = 20$, where the red, green and blue curves

correspond to $U = 0, 2$ and 3 , respectively. The reduction of current amplitude with the increase of Hubbard interaction strength is also observed for this quarter-filled case, similar to the case of half-filled as described earlier. But the point is that at quarter-filling, the reduction of current amplitude is much smaller compared to the half-filled situation. This is quite obvious in the sense that at less than half-filling ‘empty’ lattice sites are available where electrons can hop easily without any cost of extra energy and the conduction becomes much easier than the half-filled situation. In this quarter-filled case, persistent currents provide only ϕ_0 flux-quantum periodicity following the E - ϕ diagram. From these current-flux characteristics it can be concluded that for ‘ordered’ cylinders current amplitude always decreases with the enhancement in Hubbard correlation strength U .

2. Disordered cylinders with NNH integral

In order to describe the effect of impurities on electron transport now we focus our attention on the results of some typical disordered cylinders described with NNH integral. Here we consider the diagonal disordered cylinders i.e., impurities are introduced only at the site

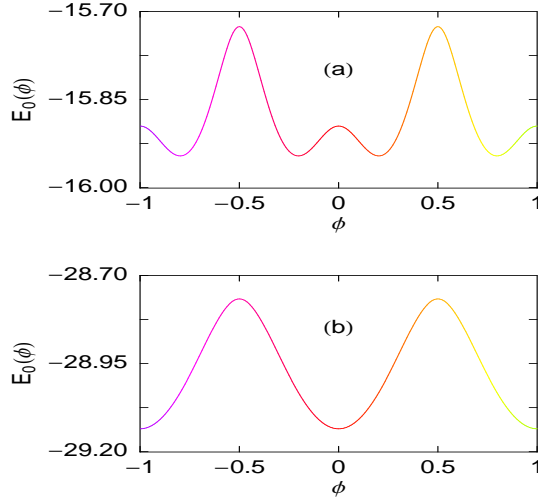


FIG. 13: (Color online). Ground state energy level as a function of flux ϕ for half-filled disordered mesoscopic cylinders ($M = 2$) considering $U = 1$ and $W = 2$. (a) $N = 5$ and (b) $N = 8$.

energies without disturbing the hopping integrals. The site energies in each concentric ring are chosen from a correlated distribution function which looks in the form,

$$\epsilon_{j,\uparrow} = \epsilon_{j,\downarrow} = W \cos(j\lambda\pi) \quad (8)$$

where, W is the impurity strength. λ is an irrational number and we choose $\lambda = (1+\sqrt{5})/2$, for the sake of our illustration. Setting $\lambda = 0$, we get back the pure system with uniform site energy W . Now, instead of considering

site energies from a correlated distribution function, as mentioned above in Eq. 8, we can also take them randomly from a ‘Box’ distribution function of width W . But in the later case we have to take the average over a large number of disordered configurations (from the stand point of statistical average) and since it is really a difficult task in the aspect of numerical computation we select the other option. Not only that in the averaging process several mesoscopic phenomena may disappear. Therefore, the averaging process is an important issue in low-dimensional systems.

In presence of disorder, energy levels get modified significantly. For our illustrative purposes in Fig. 13 we plot ground state energy levels as a function of magnetic flux ϕ for some disordered mesoscopic cylinders when they are half-filled. The Hubbard interaction strength U is set at 1 and the impurity strength W is fixed to 2. In (a) the ground state energy level is shown for a cylinder with $N = 5$ (odd), while in (b) it is presented for a cylinder taking $N = 8$ (even). Quite interestingly we see that for the cylinder with odd N , the half flux-quantum periodicity of the lowest energy level disappears in the presence of impurity and it provides conventional ϕ_0 periodicity. Hence, for cylinders with odd N , $\phi_0/2$ flux-quantum periodicity will be observed only when they are free from any impurity. For the disordered cylinder with even N ($N = 8$), the lowest energy level as usual provides ϕ_0 periodicity similar to the impurity free cylinders containing even N . Apart from this periodic nature, impurities play another significant role in the determination of the slope of the energy levels. The slope of the lowest energy level decreases significantly compared to the perfect case, and therefore, a prominent change in current amplitude also takes place.

To justify the above facts, in Fig. 14 we present the variations of persistent currents with AB flux ϕ for a half-filled mesoscopic cylinder, described in the framework of NNH model, considering $N = 15$ and $M = 2$. The red curve represents the current for the ordered ($W = 0$) non-interacting ($U = 0$) cylinder. It shows saw-tooth like nature with flux ϕ providing $\phi_0/2$ flux-quantum periodicity. The situation becomes completely different when impurities are introduced in the cylinder as seen by the other two curves. The green curve represents the current for the case only when impurities are considered but the effect of electronic correlation is not taken into account. It shows a continuous like nature with ϕ_0 flux-quantum periodicity. The most important observation is that the current amplitude gets reduced enormously, even an order of magnitude, compared to the perfect cylinder. This is due to the localization of the energy eigenstates in the presence of impurity, which is the so-called Anderson localization. Hence, a large difference exists in the current amplitudes of an ordered and disordered non-interacting cylinders and it was the main controversial issue among the theoretical and experimental predictions. Experimental verifications suggest that the measured current amplitude is quite comparable to the theoretical current

amplitude obtained in a perfect system. To remove this controversy, as a first attempt, we include the effect of e-e correlation in the disordered cylinder described by the NNH model. The result is shown by the blue curve where U is fixed at 1.5. It is observed that the current amplitude gets increased compared to the non-interacting disordered cylinder, though the increment is too small. Not only that the enhancement can take place only for small values of U , while for large enough U the current amplitude rather decreases. This phenomenon can be implemented as follows. For the non-interacting disordered

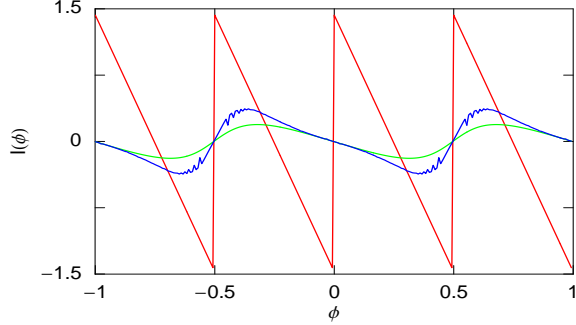


FIG. 14: (Color online). Persistent current as a function of flux ϕ for a half-filled mesoscopic cylinder considering $N = 15$ and $M = 2$. The red line corresponds to the ordered case when $U = 0$, whereas the green and blue lines correspond to the disordered case ($W = 2$) when $U = 0$ and 1.5, respectively.

cylinder the probability of getting two opposite spin electrons becomes higher at the atomic sites where the site energies are lower than the other sites since the electrons get pinned at the lower site energies to minimize the ground state energy, and this pinning of electrons becomes increased with the rise of impurity strength W . As a result the mobility of electrons and hence the current amplitude gets reduced with the increase of impurity strength W . Now, if we introduce electronic correlation in the system then it tries to depin two opposite spin electrons those are situated together due to the Coulomb repulsion. Therefore, the electronic mobility is enhanced which provides larger current amplitude. But, for large enough interaction strength, no electron can able to hop from one site to other at the half-filling since then each site is occupied either by an up or down spin electron which does not allow other electron of opposite spin due to the repulsive term U . Accordingly, the current amplitude gradually decreases with U . On the other hand, at less than half-filling though there is some finite probability to hop an electron from one site to the other available ‘empty’ site but still it is very small. So, in brief, we can say that within the nearest-neighbor hopping (NNH) approximation electron-electron interaction does not provide any significant contribution to enhance the current amplitude, and hence the controversy regarding the current amplitude still persists.

3. Disordered cylinders with NNH and SNH integrals

To overcome the existing situation regarding the current amplitude, in this sub-section, finally we make an attempt by incorporating the effect of second-neighbor hopping (SNH) integral in addition to the nearest-neighbor hopping (NNH) integral.

A significant change in current amplitude takes place when we include the contribution of second-neighbor hopping (SNH) integral in addition to the NNH integral. As representative examples, in Fig. 15 we plot the current-flux characteristics for a half-filled mesoscopic cylinder considering $N = 15$ and $M = 2$. The black, magenta

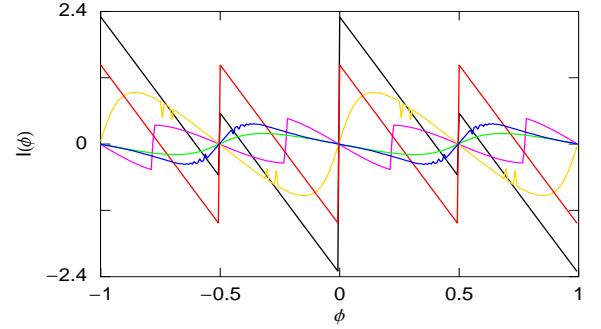


FIG. 15: (Color online). Persistent current as a function of flux ϕ for a half-filled mesoscopic cylinder taking $N = 15$ and $M = 2$ in the presence of NNH and SNH integrals. The black line corresponds to the ordered case when $U = 0$, whereas the magenta and gold lines correspond to the disordered case ($W = 2$) when $U = 0$ and 1.5, respectively. Here SNH integral is fixed at -0.6 . The currents shown by the red, green and blue lines for the ring described with NNH model (identical to Fig. 14) are re-plotted to judge the effect of SNH integral over NNH model much clearly.

and gold lines correspond to the results in the presence of SNH integral, while the other three colored curves (red, green and blue) represent the currents in the absence of SNH integral. Here we choose $t_d = -0.6$. The black curve refers to the persistent current for the perfect ($W = 0$) non-interacting ($U = 0$) cylinder and it achieves much higher amplitude compared to the NNH model (red curve). This additional contribution comes from the SNH integral since it allows electrons to hop further. In addition it is also noticed that the current varies periodically with ϕ providing ϕ_0 flux-quantum periodicity, instead of $\phi_0/2$ as in the case of NNH integral model (red curve). Thus, it can be emphasized that $\phi_0/2$ periodicity will be observed only when the cylinder is (a) free from impurity, (b) half-filled, (c) made with odd N , and (d) described by the nearest-neighbor hopping model. The main focus of this sub-section is to interpret the combined effect of SNH integral and electron-electron correlation on the enhancement of persistent current amplitude in disordered cylinder. To do this first we narrate the effect of SNH integral in disordered non-interacting cylinder. The nature of the current for this particular case is shown by the

magenta curve of Fig. 15. It shows that the current amplitude gets reduced compared to the perfect case (black line), which is expected, but the reduction of the current amplitude is quite small than the NNH integral model. This is due the fact that the SNH integral tries to delocalize the electronic states, and therefore, the mobility of the electrons is enriched. The situation becomes more interesting when we include the effect of Hubbard interaction. The behavior of the current in the presence of interaction is plotted by the gold curve of Fig. 15 where

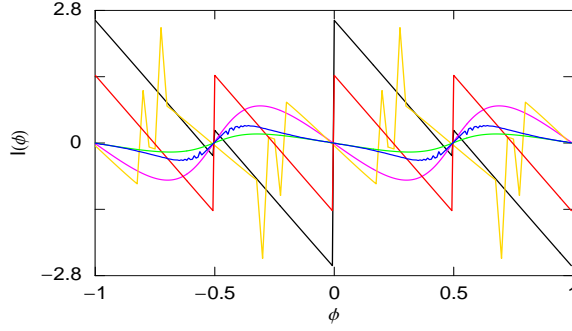


FIG. 16: (Color online). Persistent current as a function of flux ϕ for a half-filled mesoscopic cylinder taking $N = 15$ and $M = 2$ in the presence of NNH and SNH integrals. The black line corresponds to the ordered case when $U = 0$, whereas the magenta and gold lines correspond to the disordered case ($W = 2$) when $U = 0$ and 1.5 , respectively. Here SNH integral is fixed at -0.8 . The currents shown by the red, green and blue lines for the ring described with NNH model (identical to Fig. 14) are re-plotted to judge the effect of SNH integral over NNH model much clearly.

we fix $U = 1.5$. Very interestingly we see that the current amplitude is enhanced significantly and quite comparable to that of the perfect cylinder.

For better clarity of the results discussed above, in Fig. 16 we also present the similar feature of persistent current for other hopping strength of SNH integral. Here we set $t_d = -0.8$. From these curves we see that the current amplitude gets enhanced more as we increase the SNH strength.

Thus, it can be emphasized that the presence of higher order hopping integrals and electron-electron correlation may provide a persistent current which can be comparable to the measured current amplitudes. Throughout the above analysis we set the width of the cylinders at a fixed value ($M = 2$), for the sake of our illustration. But, all these results are also valid for cylinders of larger widths.

IV. A MESOSCOPIC RING WITH RASHBA AND DRESSELHAUS SO INTERACTIONS

Finally, in this section we address the magneto-transport properties in a mesoscopic ring, threaded by an AB flux ϕ , in the presence of Rashba and Dresselhaus SO interactions. We establish that the presence of SO

interaction, in general, leads to an enhanced amplitude of the persistent current. This is another one approach through which we can justify the appearance of larger current amplitude in a disordered ring. For this discussion we neglect the effect of electron-electron interaction.

A. Model, TB Hamiltonian and the theoretical formulation

The schematic view of a mesoscopic ring subjected to an AB flux ϕ (measured in unit of the elementary flux quantum $\phi_0 = ch/e$) is shown in Fig. 17. Within a TB

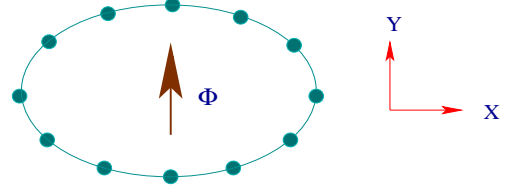


FIG. 17: (Color online). A mesoscopic ring threaded by an AB flux ϕ .

framework the Hamiltonian for such an N -site ring is⁶⁷⁻⁶⁹ (and references therein),

$$H = H_0 + H_{so}. \quad (9)$$

Here,

$$H_0 = \sum_n c_n^\dagger \epsilon_0 c_n + \sum_n (c_n^\dagger t e^{i\theta} c_{n+1} + h.c.) \quad (10)$$

and,

$$H_{so} = - \sum_n \left[c_n^\dagger t_{so} e^{i\theta} c_{n+1}^\dagger + h.c. \right] \quad (11)$$

where,

$$t_{so} = it_{Rso} (\sigma_x \cos \varphi_{n,n+1} + \sigma_y \sin \varphi_{n,n+1}) - it_{Dso} (\sigma_y \cos \varphi_{n,n+1} + \sigma_x \sin \varphi_{n,n+1}). \quad (12)$$

$n = 1, 2, \dots, N$ is the site index along the azimuthal direction φ of the ring. The other factors in Eqs. 10 and 12 are as follows.

$$c_n = \begin{pmatrix} c_{n\uparrow} \\ c_{n\downarrow} \end{pmatrix}; \epsilon_0 = \begin{pmatrix} \epsilon_0 & 0 \\ 0 & \epsilon_0 \end{pmatrix}; t = t \begin{pmatrix} 1 & 0 \\ 0 & 1 \end{pmatrix}.$$

Here ϵ_0 is the site energy of each atomic site of the ring. t is the nearest-neighbor hopping integral and $\theta = 2\pi\phi/N$ is the phase factor due to the AB flux ϕ threaded by the ring. t_{Rso} and t_{Dso} are the isotropic nearest-neighbor transfer integrals which measure the strengths of Rashba and Dresselhaus SO couplings, respectively, and $\varphi_{n,n+1} = (\varphi_n + \varphi_{n+1})/2$, where $\varphi_n = 2\pi(n-1)/N$. σ_x and σ_y are the Pauli spin matrices. $c_{n\sigma}^\dagger$ ($c_{n\sigma}$) is the creation (annihilation)

operator of an electron at the site n with spin σ (\uparrow, \downarrow). Throughout the numerical analysis, in this sub-section, we choose $t = 1$ and measure the SO coupling strength in unit of t .

At absolute zero temperature ($T = 0\text{K}$), the persistent current in the ring described with fixed number of electrons N_e is determined by,

$$I(\phi) = -c \frac{\partial E_0(\phi)}{\partial \phi} \quad (13)$$

where, $E_0(\phi)$ is the ground state energy. We compute this quantity by exactly diagonalizing the TB Hamiltonian (Eq. 9) to understand unambiguously the role of the RSOI interaction alone on persistent current.

B. Numerical results and discussion

Energy-flux characteristics: Before presenting the results for $I(\phi)$, to make the present communication a self contained study, we first take a look at the energy spectrum of both an ordered and a disordered ring with

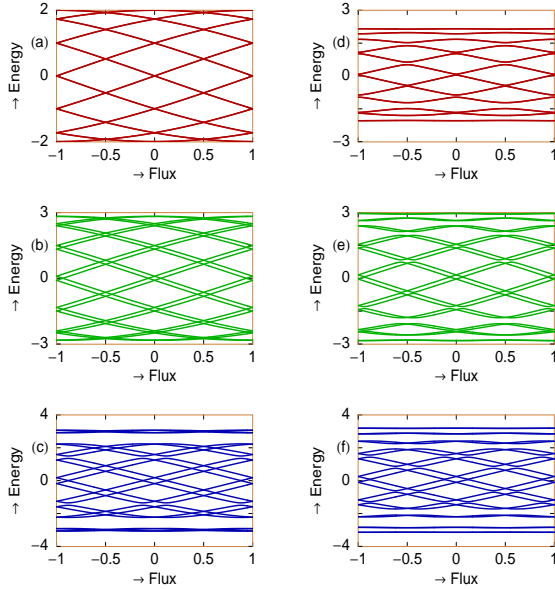


FIG. 18: (Color online). E - ϕ curves of a 12-site ring, where the 1st and 2nd columns correspond to the results for the ordered ($W = 0$) and disordered ($W = 1$) cases, respectively. The red, green and blue lines correspond to $t_{Rso} = t_{Dso} = 0$; $t_{Rso} = 1$, $t_{Dso} = 0$ and $t_{Rso} = 1$, $t_{Dso} = 0.5$, respectively.

and without the SO interactions, as the flux through the ring is varied. In Fig. 18 the flux dependent spectra are shown for a 12-site ordered ring and a randomly disordered one (with diagonal disorder) in the left and the right columns respectively. Clearly, disorder destroys the band crossings observed in the ordered case. The presence of the RSOI and the DSOI also lifts the degeneracy and opens up gaps towards the edges of the spectrum.

Enhancement of persistent current:

• **An ordered ring:** In Fig. 19 we examine the effect of the RSOI on the persistent current of an ordered ring with 80 sites. The DSOI is set equal to zero. We have examined both the non-half-filled and half-filled band cases, but present results for the latter only to save space. With increasing strength of the RSOI the persistent current

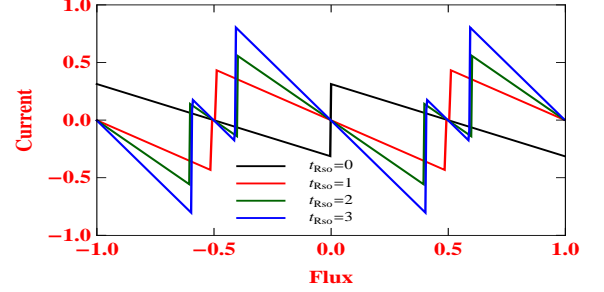


FIG. 19: (Color online). Current-flux characteristics of a 80-site ordered ($W = 0$) half-filled ring for different values of t_{Rso} when t_{Dso} is set at 0.

exhibits a trend of an increase in its amplitude. Local phase reversals take place together with the appearance of kinks in the current-flux diagrams which are however, not unexpected even without the RSOI, and are results of the band crossings observed in the spectra of such rings. The amplitude of the persistent current at a specific value of the magnetic flux is of course not predictable in any simple manner, and is found to be highly sensitive to

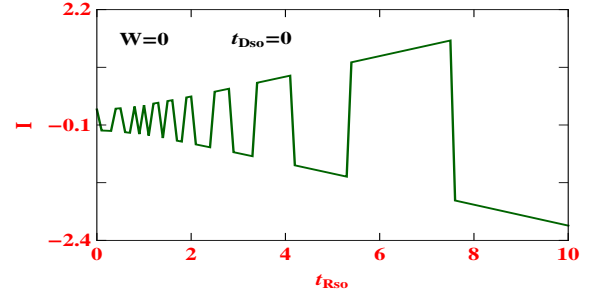


FIG. 20: (Color online). Persistent current at a particular AB flux ($\phi = 0.25$) as a function Rashba SO interaction strength for an ordered ($W = 0$) half-filled ring with $N = 60$ when t_{Dso} is set to zero.

the number of electrons N_e (i.e., the filling factor). Issues related to the dependence of the persistent current on the filling factor have been elaborately discussed by Splettstoesser *et al.*⁶⁸.

The persistent current in an ordered ring also exhibits interesting oscillations in its amplitude as the RSOI is varied keeping the magnetic flux fixed at a particular value. The oscillations persist irrespective of the band-filling factor N_e , with or without the presence of the DSOI. In Fig. 20 the oscillating nature of persistent current is presented for a 60-site ordered ring in the half-

filled band case when ϕ is set at $\phi_0/4$. The current exhibits oscillations with growing amplitude as the strength of the RSOI is increased.

- **A disordered ring:** We now present the results for a disordered ring of 80 sites in Fig. 21. Disorder is introduced via a random distribution (width $W = 2$) of the values of the on-site potentials (diagonal disorder), and results averaged over sixty disorder configurations have been presented. The DSOI remains zero. Without any

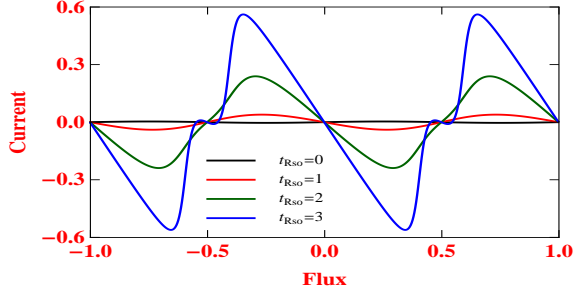


FIG. 21: (Color online). Current-flux characteristics of a 80-site disordered ($W = 2$) half-filled ring for different values of t_{Rso} when t_{Dso} is fixed at 0.

spin-orbit interaction, disorder completely suppresses the persistent current (an effect of the localization of the electronic states in the ring), as it is observed in Fig. 21 (black curve). With the introduction of the RSOI, the current starts increasing, and for $t_{Rso} = 3$ (blue curve), increases significantly, attaining a magnitude comparable

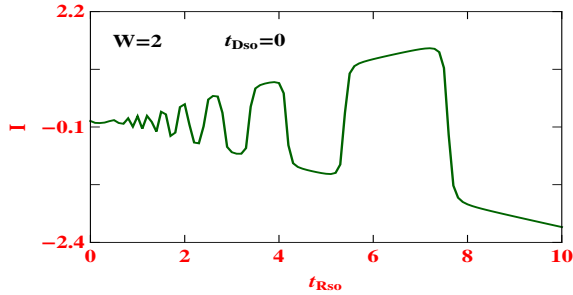


FIG. 22: (Color online). Persistent current at a particular AB flux ($\phi = 0.25$) as a function Rashba SO interaction strength for a disordered ($W = 2$) half-filled ring with $N = 60$ when t_{Dso} is set to zero.

to that in a perfectly ordered ring. It is to be noted that the strength of the RSOI is strongly dependent on gate voltage. An enhancement of the persistent current in the presence of disorder can be achieved even with much lower values of the RSOI parameter compared to what have already been presented in the figures. To achieve this one needs to increase the size of the mesoscopic ring. We have checked this with a 100-site ring where even with $t_{Rso} = 0.5$ the current increases by an order of magnitude compared to the case when $t_{Rso} = 0$. However, we present the results using a somewhat larger values of t_{Rso}

for a better viewing of the results. Similar observations are made by setting $t_{Rso} = 0$ and varying t_{Dso} .

Disorder introduces quantum interference which leads to localization of the electronic states. RSOI, on the other hand, introduces spin flip scattering in the system, which can destroy quantum interference effect, leading to a possible delocalization of the electronic states. This leads to an enhancement of the persistent current in the presence of disorder. The competition between the strength of disorder and the RSOI is also apparent in Fig. 22. For small values of the RSOI, the disorder dominates. As the strength of the RSOI is increased, the spin flip scattering starts dominating over the quantum interference effect, and finally the oscillations become quite similar to that in a ballistic ring. As the SO interaction is a natural interaction for a quantum ring grafted at a heterojunction, we are thus tempted to propose that the spin-orbit interaction is responsible for an enhanced persistent current in such mesoscopic disordered rings.

Before we end this section, we would like to mention that the presence of DSOI alone leads to exactly similar results as expected, since the Rashba and the Dresselhaus Hamiltonians are related by a unitary transformation. This does not change the physics. We also examine the behavior of persistent current in presence of both the interactions. The amplitude of the current does not increase significantly compared to the case where only one interaction is present. However, the precise magnitude of the current is sensitive to the strength of the magnetic flux threading the ring. The observation remains valid even when the strengths of the RSOI and DSOI are the same.

V. SUMMARY AND CONCLUSIONS

In this review we have demonstrated the magnetotransport properties in single-channel rings and multi-channel cylinders based on the tight-binding framework. Several anomalies between the theoretical and experimental results have been pointed out and we have tried to remove some of these discrepancies. The main controversy is associated with the proper determination of persistent current amplitude. We have addressed two different possibilities of getting enhanced current amplitudes and proved that the currents are quite comparable to the experimentally predicted results. In one approach we have concluded after an exhaustive numerical calculation that the presence of higher order hopping integrals and electron-electron interaction can provide a persistent current which may be comparable to the actual measured values. We have justified these results both for the single-channel and multi-channel cases. In other approach we have established that in presence of spin-orbit interaction a considerable enhancement of current amplitude takes place, even for the non-interacting nearest-neighbor hopping model, and the magnitude of the current in a disordered ring becomes almost comparable to that of an

ordered one. In addition to these, we have also analyzed the detailed band structures, low-field magnetic susceptibilities, variation of electronic mobility and some other issues to get the full picture of the phenomena at the meso-scale and nano-scale levels.

Here we have considered several important approximations by ignoring the effects of temperature, electron-phonon interaction, etc. Due to these factors, any scattering process that appears in the systems would have influence on electronic phases. At the end, we would like to say that we need further study in such systems by incorporating all these effects.

Future directions and opportunities: Although the studies involving the mesoscopic rings and cylinders have

already generated a wealth of literature there is still need to look deeper into the problems both from the point of view of fundamental physics and to resolve a few issues that have not yet been answered in an uncontroversial manner. For example, it may be interesting to study the combined effect of electron-electron interaction and spin-orbit interaction on magneto-transport properties. Specially, the effect of SO interaction on electron transport in mesoscopic and nano-scale semiconductor structures should be carefully examined. The principal reason is its potential application in spintronics, where the possibility of manipulating and controlling the spin of the electron rather than its charge, plays the all important role^{70–73}.

-
- * Electronic address: santanu@post.tau.ac.il
- ¹ Y. Imry, *Introduction to Mesoscopic Physics*. Oxford University Press, New York (1997).
 - ² S. Datta, *Electronic transport in mesoscopic systems*, Cambridge University Press, Cambridge (1995).
 - ³ S. Datta, *Quantum Transport: Atom to Transistor*, Cambridge University Press, Cambridge (2005).
 - ⁴ G. Metalidis, *Electronic Transport in Mesoscopic Systems*. PhD thesis, Martin-Luther-Universität Halle-Wittenberg (2007).
 - ⁵ D. Weinmann, *The Physics of Mesoscopic Systems*, (2005), based on the Lectures held during the Seventh Petra School of Physics during 17-22 September 2000 at the University of Jordon.
 - ⁶ A. Aharony, O. Entin-Wohlman, Y. Tokura, and S. Katsumoto, Phys. Rev. B **78**, 125328 (2008).
 - ⁷ A. Aharony, O. Entin-Wohlman, Y. Tokura, and S. Katsumoto, Proceedings, FQMT08.
 - ⁸ A. Rodriguez, F. Dominguez-Adame, I. Gomez, and P. A. Orellana, Phys. Lett. A **320**, 242 (2003).
 - ⁹ I. Gomez and M. L. Ladrón de Guevara, Phys. Rev. B **67**, 085321 (2003).
 - ¹⁰ A. Levy Yeyati and M. Büttiker, Phys. Rev. B **52**, R14360 (1995).
 - ¹¹ M. E. Torio, K. Hallberg, S. Flach, A. E. Miroshnichenko, and M. Titov, Eur. Phys. J. B **37**, 399 (2004).
 - ¹² E. Buks, R. Schuster, M. Heiblum, D. Mahalu, V. Umansky, and H. Shtrikman, Phys. Rev. Lett. **77**, 4664 (1996).
 - ¹³ A. Fuhrer, P. Brushein, T. Ihn, M. Sigrist, K. Ensslin, W. Wegscheider, and M. Bichler, Phys. Rev. B **73**, 205326 (2006).
 - ¹⁴ K. Kobayashi, H. Aikawa, A. Sano, S. Katsumoto, and Y. Iye, Phys. Rev. B **70**, 035319 (2004).
 - ¹⁵ M. Popp, D. Frustaglia, and K. Richter, Nanotechnology **14**, 347 (2003).
 - ¹⁶ P. Földi, O. Kalman, M. G. Benedict, and F. M. Peeters, Nano Lett. **8**, 2556 (2008).
 - ¹⁷ D. Bercioux, M. Governale, V. Cataudella, and V. M. Ramaglia, Phys. Rev. Lett. **93**, 056802 (2004).
 - ¹⁸ D. Bercioux, M. Governale, V. Cataudella, and V. M. Ramaglia, Phys. Rev. B **72**, 075305 (2005).
 - ¹⁹ J. Vidal, B. Doucot, R. Mosseri, and P. Butaud, Phys. Rev. Lett. **85**, 3906 (2000).
 - ²⁰ B. Doucot and J. Vidal, Phys. Rev. Lett. **88**, 227005 (2002).
 - ²¹ S. K. Maiti, J. Phys. Soc. Jpn. **78**, 114602 (2009).
 - ²² S. K. Maiti, Phys. Lett. A **373**, 4470 (2009).
 - ²³ S. K. Maiti, Solid State Commun. **149**, 1623 (2009).
 - ²⁴ M. Büttiker, Y. Imry, and R. Landauer, Phys. Lett. **96A**, 365 (1983).
 - ²⁵ L. P. Levy, G. Dolan, J. Dunsmuir, and H. Bouchiat, Phys. Rev. Lett. **64**, 2074 (1990).
 - ²⁶ V. Chandrasekhar, R. A. Webb, M. J. Brady, M. B. Ketchen, W. J. Gallagher, and A. Kleinsasser, Phys. Rev. Lett. **67**, 3578 (1991).
 - ²⁷ D. Mailly, C. Chapelier, and A. Benoit, Phys. Rev. Lett. **70**, 2020 (1993).
 - ²⁸ E. M. Q. Jariwala, P. Mohanty, M. B. Ketchen, and R. A. Webb, Phys. Rev. Lett. **86**, 1594 (2001).
 - ²⁹ R. Deblock, R. Bel, B. Reulet, H. Bouchiat, and D. Mailly, Phys. Rev. Lett. **89**, 206803 (2002).
 - ³⁰ B. Reulet, M. Ramin, H. Bouchiat, and D. Mailly, Phys. Rev. Lett. **75**, 124 (1995).
 - ³¹ H. F. Cheung, Y. Gefen, E. K. Riedel, and W. H. Shih, Phys. Rev. B **37**, 6050 (1988).
 - ³² H. F. Cheung and E. K. Riedel, Phys. Rev. Lett. **62**, 587 (1989).
 - ³³ L. K. Castelano, G.-Q. Hai, B. Partoens, and F. M. Peeters, Phys. Rev. B **78**, 195315 (2008).
 - ³⁴ M. Zarenia, M. J. Pereira, F. M. Peeters, and G. de Farias, Phys. Rev. B **81**, 045431 (2010).
 - ³⁵ D. Y. Vodolazov, F. M. Peeters, T. T. Hongisto, and K. Yu. Arutyunov, Europhys. Lett. **75**, 315 (2006).
 - ³⁶ G. Montambaux, H. Bouchiat, D. Sigeti, and R. Friesner, Phys. Rev. B **42**, 7647 (1990).
 - ³⁷ H. Bouchiat and G. Montambaux, J. Phys. (Paris) **50**, 2695 (1989).
 - ³⁸ B. L. Altshuler, Y. Gefen, and Y. Imry, Phys. Rev. Lett. **66**, 88 (1991).
 - ³⁹ F. von Oppen and E. K. Riedel, Phys. Rev. Lett. **66**, 84 (1991).
 - ⁴⁰ A. Schmid, Phys. Rev. Lett. **66**, 80 (1991).
 - ⁴¹ V. Ambegaokar and U. Eckern, Phys. Rev. Lett. **65**, 381 (1990).
 - ⁴² M. Abraham and R. Berkovits, Phys. Rev. Lett. **70**, 1509 (1993).
 - ⁴³ G. Bouzerar, D. Poilblanc, and G. Montambaux, Phys. Rev. B **49**, 8258 (1994).

- ⁴⁴ T. Giamarchi and B. S. Shastry, Phys. Rev. B **51**, 10915 (1995).
- ⁴⁵ N. Yu and M. Fowler, Phys. Rev. B **45**, 11795 (1992).
- ⁴⁶ S. Bellucci and P. Onorato, Physica E **41**, 1393 (2009).
- ⁴⁷ P. A. Orellana and M. Pacheco, Phys. Rev. B **71**, 235330 (2005).
- ⁴⁸ H.-M. Li and J.-L. Xiao, Physica B **396**, 91 (2007).
- ⁴⁹ H.-M. Li, Y.-L. Huang, and J.-L. Xiao, Int. J. Mod. Phys. B **22**, 2255 (2008).
- ⁵⁰ S. K. Maiti, Physica E **31**, 117 (2006).
- ⁵¹ S. K. Maiti, Solid State Phenomena **155**, 87 (2009).
- ⁵² S. K. Maiti, S. Saha, and S. N. Karmakar, Eur. Phys. J. B **79**, 209 (2011).
- ⁵³ S. K. Maiti, J. Appl. Phys. **110**, 064306 (2011).
- ⁵⁴ H. Bluhm, N. C. Koshnick, J. A. Bert, M. E. Huber, and K. A. Moler, Phys. Rev. Lett. **102**, 136802 (2009).
- ⁵⁵ W. Rabaud, L. Saminadayar, D. Mailly, K. Hasselbach, A. Benoit, and B. Etienne, Phys. Rev. Lett. **86**, 3124 (2001).
- ⁵⁶ L. Meier, G. Salis, I. Shorubalko, E. Gini, S. Schön, and K. Ensslin, Nature Physics **3**, 650 (2007).
- ⁵⁷ J. Premper, M. Trautmann, J. Henk, and P. Bruno, Phys. Rev. B **76**, 073310 (2007).
- ⁵⁸ H. Kato and D. Yoshioka, Phys. Rev. B **50**, 4943 (1994).
- ⁵⁹ A. Kambili, C. J. Lambert, and J. H. Jefferson, Phys. Rev. B **60**, 7684 (1999).
- ⁶⁰ S. K. Maiti and A. Chakrabarti, Phys. Rev. B **82**, 184201 (2010).
- ⁶¹ S. K. Maiti, Solid State Commun. **150**, 2212 (2010).
- ⁶² S. K. Maiti, Phys. Status Solidi B **248**, 1933 (2011).
- ⁶³ S. K. Maiti, M. Dey, S. Sil, A. Chakrabarti, and S. N. Karmakar, Europhys. Lett. **95**, 57008 (2011).
- ⁶⁴ W. Kohn, Phys. Rev. **133**, A171 (1964).
- ⁶⁵ B. S. Shastry and B. Sutherland, Phys. Rev. Lett. **65**, 243 (1990).
- ⁶⁶ H. Shiba, Phys. Rev. B **6**, 930 (1972).
- ⁶⁷ J. S. Sheng and K. Chang, Phys. Rev. B **74**, 235315 (2006).
- ⁶⁸ J. Splettstoesser, M. Governale, and U. Zülicke, Phys. Rev. B **68**, 165341 (2003).
- ⁶⁹ C. P. Moca and D. C. Marinescu, J. Phys.: Condens. Matter **18**, 127 (2006).
- ⁷⁰ I. Zutic, J. Fabian, and S. Das Sarma, Rev. Mod. Phys. **76**, 323 (2004).
- ⁷¹ G.-H. Ding and B. Dong, Phys. Rev. B **76**, 125301 (2007).
- ⁷² S. Bellucci and P. Onorato, Phys. Rev. B **78**, 235312 (2008).
- ⁷³ M. Dey, S. K. Maiti, and S. N. Karmakar, J. Appl. Phys. **109**, 024304 (2011).